Widespread inundation of Pacific islands triggered by distant-source wind-waves ☆

CrossMark

Ron K. Hoeke [a,*], Kathleen L. McInnes [a], Jens C. Kruger [b], Rebecca J. McNaught [c], John R. Hunter [d,f], Scott G. Smithers [e]

[a] CSIRO Marine and Atmospheric Research, Australia
[b] SPC Applied Geoscience and Technology Division, Fiji
[c] Red Cross/Red Crescent Climate Centre, Vanuatu
[d] Antarctic Climate & Ecosystems Cooperative Research Centre, Australia
[e] James Cook University, Australia
[f] University of Tasmania, Australia

ABSTRACT

It is essential to understand the causes of sea level extremes in order to anticipate and respond to coastal flooding (inundation), and to adapt to sea level rise. We investigate a series of inundation events which occurred across the western Pacific over several consecutive days during December 2008, causing severe impacts to five Pacific Island nations. These events were not associated with commonly identified causes: tropical cyclones or unusually large astronomical tides. Instead, the dissipation of wind-waves generated by distant extra-tropical cyclones (swell) was the main cause, although regional sea level variability, including recent accelerated rise, significantly contributed to the severity of impact experienced at many locations. The implication of recent sea level rise in the severity of these events suggests that episodic swell will increasingly cause major impacts of the nature described herein, although such impacts will continue to be modulated by El Niño/Southern Oscillation (ENSO) variability in the region. Significantly, tide gauges recorded little evidence of extreme sea levels during the event, implying that causes of extreme sea levels inferred from tide gauge analysis are unlikely to include this important cause of inundation. Therefore, any assessment of inundation risk predicated on tide gauge information (as well as larger scale sea level information such as satellite altimetry) may fail at many locations in the Pacific. To be accurate, such efforts must include information on the relationship between wave climate, wave forecasts and local extreme water levels. Further development of related early warning systems will become more pertinent as modern SLR continues to add to the magnitude of extremes.

© 2013 The Authors. Published by Elsevier B.V. All rights reserved.

1. Introduction

More frequent and severe inundation associated with climate-change related sea level rise (SLR) is one of the biggest threats to coastal communities and particularly island nations (Nicholls et al., 2007; Seneviratne et al., 2012). Inundation events can significantly change shorelines, damage infrastructure, contaminate freshwater reserves, destroy food crops, and in the severest of cases, take human lives (Barnett, 2011). Higher mean sea levels will exacerbate the impacts of extreme sea levels caused by a range of other processes. Understanding the processes that cause extreme sea levels and subsequent inundation is of paramount importance to climate change adaptation strategies of island nations.

It has long been recognized that long-wavelength wind-waves (swell) produced by mid-latitude storms can propagate across entire ocean basins, sometimes to distances greater than 20,000 km (Munk et al., 1963; Delpey et al., 2010). Wave set-up, or the elevation of the mean still water surface due to the breaking (dissipation) of wind waves (Longuet-Higgins and Stewart, 1964), can reach approximately 1/3 of incident wave height along coasts typical of tropical and sub-tropical islands (Munk and Sargent, 1948; Tait, 1972; Vetter et al., 2010), and therefore has the potential to be a significant driver of extreme sea levels along these coastlines. Additionally, swell dissipation typically generates infra-gravity waves (e.g. Pomeroy et al., 2012) and causes uprush of individual waves at the shoreline (wave run-up), which may have considerable coastal impact. This suggests that the arrival of such swells may be a trigger of inundation events along such coasts. However, despite some evidence that this is the case (Harangozo, 1992), peer-reviewed literature on swell-driven

* Corresponding author at: 107-121 Station St, Aspendale, Victoria 3195, Australia. Tel.: +61 3 9239 4653; fax: +61 3 9239 4444.
E-mail address: ron.hoeke@csiro.au (R.K. Hoeke).
URL: http://www.cmar.csiro.au/sealevel (R.K. Hoeke).

contributions to extreme sea levels and associated coastal impacts is extremely limited: more commonly cited causes are astronomical tides, tropical cyclone storm surges and regional sea level variability such as that due to El Niño/Southern Oscillation (ENSO), e.g. Church et al. (2006), Lowe et al. (2010), Menèndez and Woodworth (2010) and Walsh et al. (2012). Contributing reasons for the scant literature addressing swell as a cause of extreme sea level events likely include the relative remoteness of island communities, relatively poor reporting networks (OCHA, 2011; Kruke and Olsen, 2012), and the low density of in situ observations of coastal sea level and surface waves (Lowe et al., 2010). The greater importance of wind set-up and inverse barometric pressure (collectively referred to as storm surge) relative to wave set-up along better studied (and instrumented) continental shelves (Kennedy et al., 2012; Walsh et al., 2012) may also have led to the (mis)conception that coastal inundation processes are relatively well predicted and well understood for island communities. Another significant factor, as we show here, is that the tide gauge network, which is the primary data source for extreme sea level analysis (e.g. Menéndez and Woodworth, 2010), may completely miss or at least under-represent the contribution of swell to extreme sea levels.

Here, we document the environmental context and impacts surrounding a series of major inundation events, which occurred in the western Pacific during December 2008. We draw on data from a variety of sources, including newspaper articles, regional humanitarian situation reports and available meteorological and oceanographic data and reanalysis products. Most reports suggest that significant inundation occurred over several consecutive days at high tide, with several reports indicating additional impacts due to wave run-up and infra-gravity bores "surging" across low-lying islands. The reports indicate widespread and severe damage to infrastructure and key natural resources such as soils and freshwater at islands in Micronesia, the Marshall Islands, Kiribati, Papua New Guinea and the Solomon Islands. We show that a large, though not unique, swell generated in the mid-latitude regions of the northern Pacific Ocean, more than 4000 km from the furthest affected island, was the main cause of these damaging events, but that regionally elevated sea level, due to both La Nina conditions and non-ENSO SLR, also played an important role.

2. Data sources and derived information

2.1. Inundation reports

Reports of inundation were collated from a variety of sources including; the United Nations Office for the Coordination of Humanitarian Affairs (http://www.unocha.org/) Situation Reports database, the International Federation of Red Cross and Red Crescent Societies (http://www.ifrc.org/) Disaster Management Information System (DMIS) database, the Pacific Disaster Net database (http://www.pacificdisaster.net/), the U.S. Federal Emergency Management Agency (http://www.fema.gov/), as well as reports from disaster management and meteorological agencies of the island countries and personal interviews (see Supplementary Table S1 for a summary of all reports). Information contained within the reports varied widely and significant interpretation was required, e.g. level of impact was sometimes difficult to ascertain and actual inundation may have occurred somewhat earlier than reported, given the remote location of the events (Kruke and Olsen, 2012). Despite these challenges, the date, time, maximum water level and overall damage of the inundation reported at each location were ascertained as objectively as possible and converted to UTC time to allow comparison with geophysical data. We classified the reported inundation impacts (or lack thereof) as following:

(1) None: no reported damage
(2) Minor: some reported damage to homes and/or limited evacuation

(3) Major: reported crop losses up to 50% and/or damage to infrastructure and/or more widespread damage to homes and some degree of community displacement
(4) Severe: reported crop losses greater than 50% and/or significant overtopping/overwashing of islands and/or displacement of large portions of entire communities.

Inundation and coastal impacts were often reported for multiple locations within single reports, sometimes encompassing vast areas (for instance, all of West Sepik, New Ireland and Bougainville provinces in Papua New Guinea (PNG), the east–west extent of which is approximately 1700 km). For simplicity, however, we report wave, sea level and meteorological information for a smaller number of "representative" locations, based primarily on proximity to geophysical data (e.g. tide gauges). These representative locations are not always in the immediate vicinity of affected locations. For instance, at locations such as Wake, Kwajalein and Majuro atolls, a tide gauge is located within the lagoon of the affected islands. In the Solomon Islands (SI) however, the Honiara tide gauge is the closest gauge to the affected atolls of Ontong Java and Sikaiana, which are several hundred kilometers north east, respectively; we therefore use Honiara as a "representative" location, despite Honiara itself being unaffected (this is something of an extreme case in the analysis). For conciseness then, we use the place or country name or acronym when discussing general reported inundation impacts, but use the representative location (based on proximity to geophysical data) or its 4-letter code when discussing actual geophysical values. For example, we use Papua New Guinea (or PNG) when discussing the event's impact on the country, but use Takuu (TAKU) or Lombrum (LOMB) when discussing or plotting tidal or wave height values for two representative locations within in PNG. See Table 1 for further clarification.

2.2. Tides

Hourly tide gauge data from the University of Hawaii Sea Level Center (http://uhslc.soest.hawaii.edu/) and the Australian Bureau of Meteorology's South Pacific Sea Level and Climate Monitoring Project (http://www.bom.gov.au/pacificsealevel/) were sourced for most locations listed in Table 1. Prior to analysis, tide gauge water levels were adjusted to a zero bias with respect to a global sea-surface height reconstruction (*SSHR*, see next section) at each location. A common datum of zero mean between the years 1990 and 1995 (a period with relatively minimal ENSO extremes) was used for both tide gauge water levels and *SSHR*. Harmonic analysis and prediction using exact nodal/satellite corrections were carried out using Utide software (Codiga, 2011). Non-tidal residuals were calculated by subtracting the resulting predicted tidal time-series from the (datum adjusted) observations. Predicted tidal heights in Table 1 are given relative to a Mean Higher High Water (MHHW) datum, defined as the mean of the highest daily tide for an 18.6-year period at each location. This makes comparison with other water level drivers easier, as the predicted highest tides are relative to an average high tide.

Water level observations for Takuu Atoll (PNG) were derived from a pressure sensor deployed in the lagoon for 22 days, fortuitously during the inundation event. The water level observations' datum was adjusted by minimizing bias between predicted tides and the observations when sea level anomaly and wave heights were at a minimum during the observation period. Tidal predictions for Takuu and for Kosrae (FSM) were made using the most current version available of the TPXO global tidal model (Egbert and Erofeeva, 2002); version 7.2 (http://volkov.oce.orst.edu/tides/).

2.3. Regional sea level, pressure and winds

A monthly gridded (1° × 1°) sea-surface height reconstruction (*SSHR*) for years 1950–2010 (Church et al., 2004; Church and White,

2011), to which no inverse barometer effect (*IBE*) adjustment has been made (i.e. *IBE* has not been subtracted from the heights), was used to examine regional sea level variation at representative locations. At each location affected, trends were calculated using a quadratic fit. Also, exceedence probabilities of regional sea level above thresholds associated with the 2008 event and corresponding return intervals were calculated empirically, i.e. through ranking the monthly values rather than fitting to a distribution. These exceedence probabilities were calculated for *SSHR* both with and without the trend removed. The *SSHR*, rather than satellite altimetry or individual tide gauges, was used as it provided continuous data over the entire period of the numerical wave hindcast (see Section 2.4), avoiding issues with data gaps and local water level effects on the tide gauges.

The satellite altimetry AVISO delayed-time gridded ($1/3° \times 1/3°$) sea-level anomaly weekly product (DT-MSLA "Ref", http://www.aviso.oceanobs.com/, referred to as *SLA* hereafter) was used to examine regional sea level variation at higher spatial and temporal resolution across the region during the event, including the maximum *SLA* indicated in Table 1. This *SLA* product has tidal and *IBE* corrections applied (a necessary step for homogenization of data from different satellites); therefore *IBE* must be added back for comparison with *SSHR*. The Climate Forecast System Re-analysis (hourly $1/3°$ spatial resolution, CFSR (Saha et al., 2010)) pressure fields were used to calculate the time and space-varying *IBE* contribution to sea level and examine the correspondence between *IBE* and the recorded inundation events. *IBE* was calculated according to:

$$IBE = \frac{P_{ref} - P}{\rho g}$$

where $P_{ref} = 101,325$ Pa and P, g and ρ are local sea-surface pressure, gravitational acceleration and mean density of seawater, respectively. CFSR wind fields at 10-m elevation were used to examine winds and the potential for local wind set-up as contributing to the reported inundation events.

Correlations between *SSHR* and monthly average and combined *SLA* and *IBE* (*SLA + IBE*, calculated for years 1992–2010) are >0.8 at all representative locations except Majuro, Nauru and Wake (see Table 1 for location definitions), where they are 0.6, 0.5 and 0.3 respectively. These latter locations also have low correlation between *SSHR* (and *SLA + IBE*) and the monthly multivariate ENSO index (MEI, Wolter and Timlin, 1998), indicating that the empirical orthogonal functions used to construct *SSHR* (Church and White, 2011) are not as representative of observed sea levels at these locations relative to the others. However elevated regional sea level did not play a large role at these locations as at other locations suffering major or severe impacts (see Section 3); this is not coincidental since ENSO does not have such an
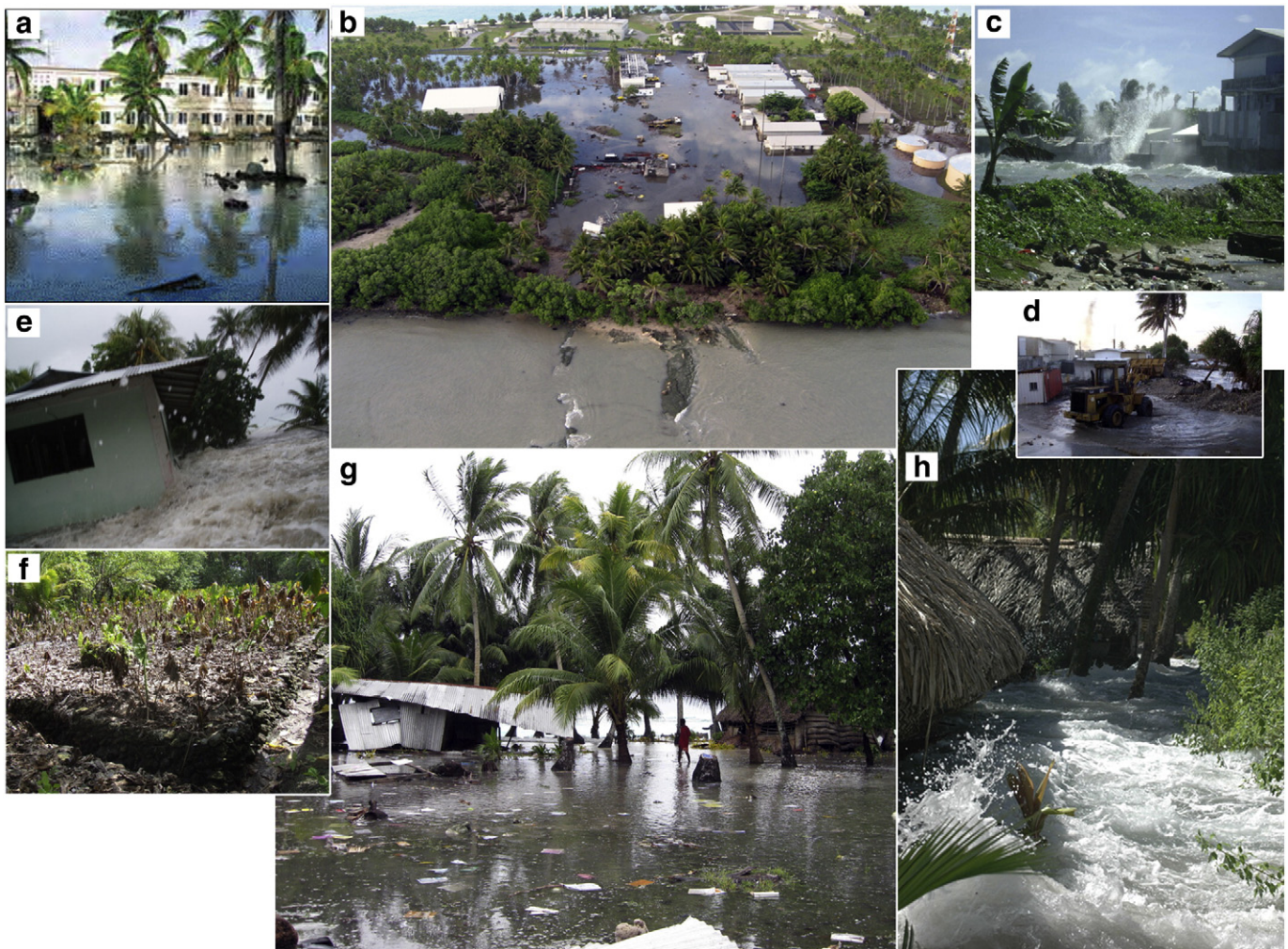

Fig. 1. Examples of the inundation events of the western Pacific during December 2008: flooded military infrastructure at (a) Wake Atoll (photo credit: Hickam Kukini/Honolulu Advertiser) and (b) Roi-Namur, Kwajalein Atoll, Marshall Islands on December 7 (photo credit: Neil Schwanitz); (c) impacts to houses (photo credit: Reginald White) and (d) emergency shoreline remediation (photo credit: Marshall Islands Journal) at Delap, Majuro Atoll, Marshall Islands on December 7; (e) wave run-up impacting houses in Kosrae State on December 8 and (f) saltwater-damaged taro crops resulting from December inundation in Chuuk State, Federated States of Micronesia (photo credit: Kosrae Resource Management Agency); (g) destroyed structures (photo credit: Scott Smithers) and (h) waves washing through the village (photo credit: Jeffrey Holdaway) at Nukutoa, Takuu Atoll, Papua New Guinea on December 10.

effect on local sea level at these locations. Furthermore, differences between December 2008 values of SSHR and SLA + IBE are less than 3 cm at all locations except Wake. We therefore use exceedence probabilities from SSHR and SLA + IBE observed during the December 2008 interchangeably, although caution should be used at Wake, and to a lesser degree, Nauru and Majuro. Similar to the tide gauge water

Table 1
Summary of water level drivers at representative locations and inundation severity reported for neighboring areas. Column one ("Loc") gives the four letter codes of the representative locations used in Figs. 2 and 3. All dates and times are given in UTC. The "Date" column indicates the day of December and hour (if know) in which inundation was first reported in neighboring areas; the asterisks following the location names ("Location" column) indicates the estimated severity: one for minor, two for major, three for severe, and none for no reported inundation. The following columns indicate maximum (peak value over the calendar month of December 2008) and the day and hour at which the maximum value occurred in parentheses. These values include predicted tide, observed water level residual, sea level anomaly (SLA), inverse barometer effect (IBE), wind magnitude, and estimated breaking wave height (H_b). The columns following H_b include peak wave period (T_p), and peak wave direction (D_p) associated with time of peak H_b. The values of T_p and D_p in parentheses indicate the largest deviation from the value associated with peak $H_b \pm 3$ h.

Loc	Location	Date	Max. predicted tide (m)	Max. observed resid. (m)	Max. SLA (m)	Max. IBE (m)	Max. Wind (m/s)	Max. H_b (m)	T_p (s)	D_p (°N)	Est. Max. Setup (m)
Wake	Wake, USA Trust***	Dec07 04h	0.213 (Dec14 05h)	0.122 (Dec05 14h)	-0.025 (Nov26)	-0.010 (Dec06 17h)	17.0 (Dec08 06h)	9.23 (Dec07 06h)	16.1 (18.2)	21 (331)	1.9
Guam	Guam, USA Terr.		0.059 (Dec14 00h)	0.324 (Dec11 13h)	0.137 (Dec10)	0.066 (Dec11 06h)	14.3 (Dec11 14h)	4.95 (Dec08 23h)	15.4 (18.5)	46 (34)	1.0
Kwaj	Kwajalein, Marshall Islands***	Dec07	0.348 (Dec13 05h)	0.308 (Dec06 09h)	0.055 (Nov26)	0.019 (Dec08 04h)	11.2 (Dec13 18h)	6.05 (Dec08 03h)	16.7 (19.2)	7 (351)	1.2
Maju	Majuro, Marshall Islands**	Dec08	0.357 (Dec13 05h)	0.164 (Dec19 00h)	0.027 (Dec10)	0.017 (Dec08 02h)	10.8 (Dec13 15h)	5.43 (Dec08 07h)	16.7 (20.0)	354 (343)	1.1
Truk	Chuuk, Micronesia**	Dec07	0.263 (Dec13 05h)		0.102 (Dec10)	0.029 (Dec10 06h)	9.9 (Dec07 22h)	5.06 (Dec07 23h)	16.7 (18.9)	25 (27)	1.0
Pohn	Pohnpei, Micronesia**	Dec07	0.255 (Dec14 05h)	0.357 (Dec18 23h)	0.089 (Dec03)	0.027 (Dec09 06h)	8.7 (Dec09 22h)	5.4 (Dec08 00h)	16.9 (18.2)	16 (22)	1.1
Kosr	Kosrae, Micronesia**	Dec07	0.38 (Dec13 05h)		0.080 (Dec17)	0.022 (Dec09 06h)	8.9 (Dec01 07h)	5.01 (Dec07 22h)	17.5 (18.2)	4 (356)	1.0
Kapi	Kapinga-marangi, Micronesia***	Dec08	0.519 (Dec13 05h)	0.268 (Dec19 14h)	0.020 (Dec10)	0.020 (Dec14 03h)	8.3 (Dec19 19h)	4.88 (Dec08 19h)	16.7 (20.0)	353 (345)	1.0
Tara	Tarawa, Kiribati*	Dec09 11h	0.302 (Dec13 05h)	0.479 (Dec09 09h)	0.086 (Dec24)	0.026 (Dec09 06h)	7.3 (Dec10 23h)	4.4 (Dec08 10h)	17.2 (19.6)	17 (24)	0.9
Naur	Nauru		0.438 (Dec13 05h)	0.291 (Dec11 03h)	0.000 (Dec17)	0.024 (Dec14 03h)	7.0 (Dec10 21h)	3.98 (Dec08 15h)	17.2 (19.2)	1 (358)	0.8
Lomb	Lobrum, Manus, Papua New Guinea***	Dec08	0.078 (Dec12 05h)	0.216 (Dec19 11h)	0.078 (Dec24)	0.025 (Dec10 06h)	7.4 (Dec11 08h)	3.9 (Dec09 10h)	16.4 (20.0)	28 (28)	0.8
Taku	Takuu, Papua New Guinea***	Dec10 02h	0.398 (Dec13 05h)	0.424 (Dec10 07h)	0.092 (Dec10)	0.032 (Dec10 05h)	7.0 (Dec11 07h)	4.18 (Dec09 00h)	17.2 (18.5)	13 (17)	0.8
Honi	Honiara, Solomon Islands**	Dec09	0.141 (Dec14 05h)	0.073 (Dec15 11h)	0.124 (Dec24)	0.033 (Dec10 04h)	9.0 (Dec10 21h)	3.79 (Dec09 08h)	16.9 (18.2)	7 (3)	0.8

Note that predicted tide is given relative to mean higher high water (MHHW). SLA is from weekly values (centered on date indicated). All values other than SLA are hourly.

levels, the sea level variables used here are adjusted to a common datum such that *SSHR* for years 1990–1995 (a period of relatively low ENSO variability with good tide gauge data availability) has mean value of zero. Further comparison of *SSHR* and *SLA + IBE* is given in Supplementary Table S2.

2.4. Waves

In situ wind-wave observations do not exist in the area affected and therefore are not available for the 2008 event. Numerical hindcasts provide the only source of continuous wind-wave information of the event itself and also are the only data sufficient to develop wind-wave climatology information (satellite altimetry observations being too sparse spatially and temporally). Significant wave height (H_s), peak period (T_p) and peak direction (D_p) fields from a 30-year hindcast (Hemer et al., 2013) were used to investigate wind-wave conditions for the December 2008 event and to establish the climatological context of the event. The hindcast utilizes the WaveWatch III numerical model (Tolman, 2009) with atmospheric forcing provided by CFSR from 1979 through 2010. Satellite altimetry observations of H_s and hindcast H_s in the western Pacific during December 5, 2008 to December 11, 2008 are highly correlated (correlation coefficient of 0.94 and a mean normalized bias of 1.2%), indicating that there is good agreement between the (sparse) altimetry observations and the hindcast (Supplementary Information S4). We also calculate two additional quantities, wave energy flux (EC_g), since this has been shown to scale with wave set-up at coral reefs (Vetter et al., 2010; Aucan et al., 2012), and maximum breaking wave height (H_b). We estimate EC_g according to linear wave theory's deepwater assumptions for group velocity (C_g) of random waves (Dean and Dalrymple, 1984):

$$E \cdot C_g = \frac{\rho g}{8} H_0^2 \cdot \frac{g}{4\pi} T$$

where g and ρ are gravitational acceleration and mean density of seawater, respectively. H_b is estimated by the numerical solution of:

$$H_b = H_0 \left(\frac{C_{g0}}{C_{gb}}\right)^{1/2}, h_b = \frac{H_b}{\gamma}$$

where H_0, C_{g0}, and C_{gb} are deepwater wave height, deepwater group velocity and group velocity at breaking, respectively. Thus H_b is a simple relation based on the conservation of onshore EC_g and the depth of breaking (h_b) is proportional to H_b according to the "breaker coefficient" γ, i.e. wave height increases as water depth and C_g decrease according to the dispersion relation (Dean and Dalrymple, 1984; Holthuijsen, 2007) up until a critical break point determined by the ratio of water depth to wave height (γ), after which energy is dissipated. Hindcast H_s and T_p values are used for H_0 and wave period (T), respectively, and a value of 1 for γ is used, which has been shown to be appropriate for coral reefs (Filipot and Cheung, 2012). This simple relation for H_b, neglects a number of processes, among them that waves travel normal to shore, which is not always the case. In reality, different angles of incidence and refraction typically lead to local increases or decreases in wave height. Also bed-friction, which has been shown to be important over reefs (Lowe et al., 2005) and tends to decrease wave heights before breaking in some situations, is ignored. These processes, which depend on localized reef morphology and sea bed types, generally result in a large range of actual breaking wave heights at any given time and location. However, H_b does provide an easily conceptualized and intercomparable metric of overall wave energy available for wave set-up and run-up processes (e.g. Caldwell and Aucan, 2007). Finally, maximum wave set-up at coral reefs has been shown to be on the order 15–30% of breaking wave height (Munk and Sargent, 1948; Tait, 1972; Vetter et al., 2010). To estimate wave set-up we simply scale H_b by 20%, a central, if somewhat conservative measure of these estimates. More rigorous analytical (e.g. Gourlay and Colleter, 2005; Lowe et al.,
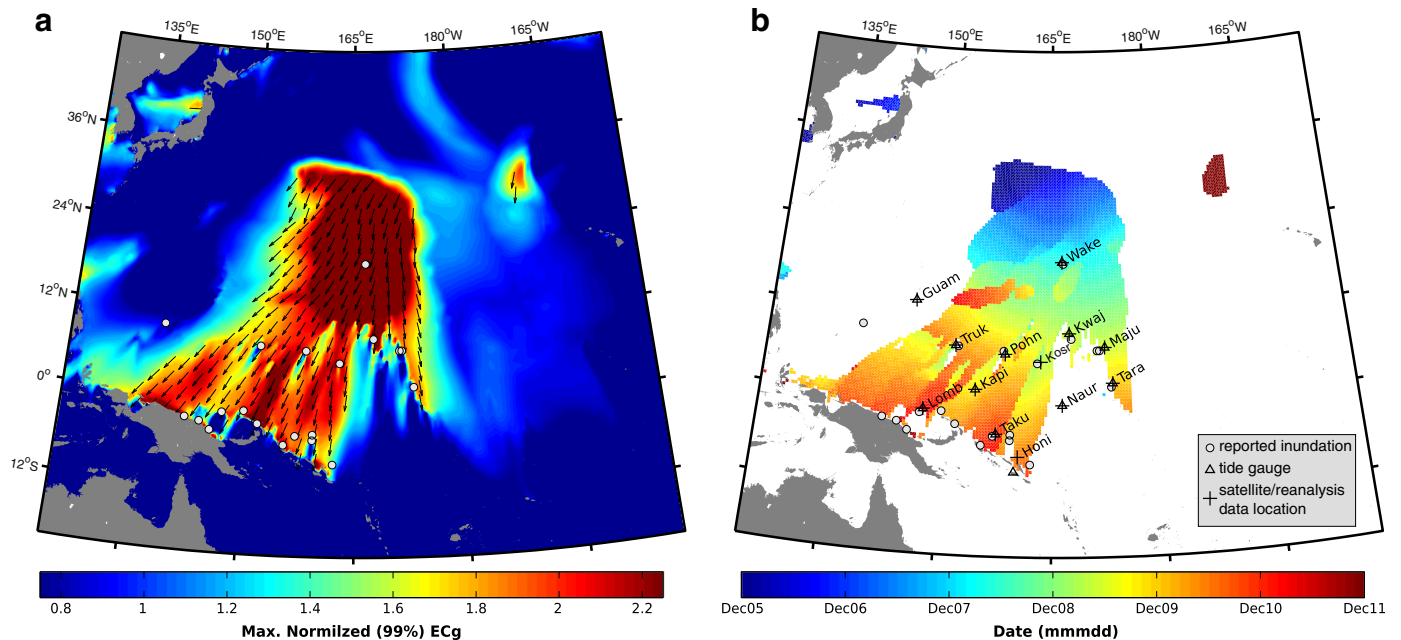

Fig. 2. (a) Maximum (peak value during the calendar month of December 2008) wave energy flux (EC_g) normalized by the 99-percentile climatology in the western Pacific with black arrows indicating peak wave direction (D_p) coincident with maximum EC_g when values are greater than 1.25 times the 99-percentile value. (b) Date/time of occurrence of maximum hindcast EC_g during December 2008 (for values greater than 1.25 times the 99-percentile value); date ticks on the color bar below indicate the start of the day (00 h UTC) in mmmdd format. In both subplots, locations with reported inundation for this period, also given in Table 1, are indicated with white circles; locations of tide gauges and other data are also given.

2009; Vetter et al., 2010) or numerical estimations (e.g. Callaghan et al., 2006; Pomeroy et al., 2012; Taebi et al., 2012) would require high-resolution bathymetric information, which is unavailable at almost all affected locations.

To put the December 2008 event into perspective, we also apply a peaks-over-threshold method to calculate empirical return intervals (RIs) of large H_b events. These events were defined as H_b event maxima (de-clustered using a 12-hour window) greater than the 99-percentile threshold. This threshold was selected since the generalized Pareto distribution shape parameter appeared to be stable in all cases near this value. The Pareto distribution was then fitted to the resulting RIs and H_b event maxima using the maximum-likelihood method at each inundation report location. To find the return-interval of the co-occurrence

of elevated regional sea level and H_b, the same method was followed, but we only considered H_b events occurring when the $SSHR$ was greater than the December 2008 event (i.e. close to the $SLA + IBE$, Table 1) minus 0.05 m. The 0.05 m is an error estimate, calculated as approximately one half the mean standard deviation of $SSHR$ across the region.

3. Chronology of events, impacts and environmental context

A review of reports on the event (listed in Supplementary Table S1) indicates the onset of inundation occurred at multiple locations across the western tropical Pacific between December 7 and December 9, 2008 (UTC time). On December 7, inundation occurred on the northern
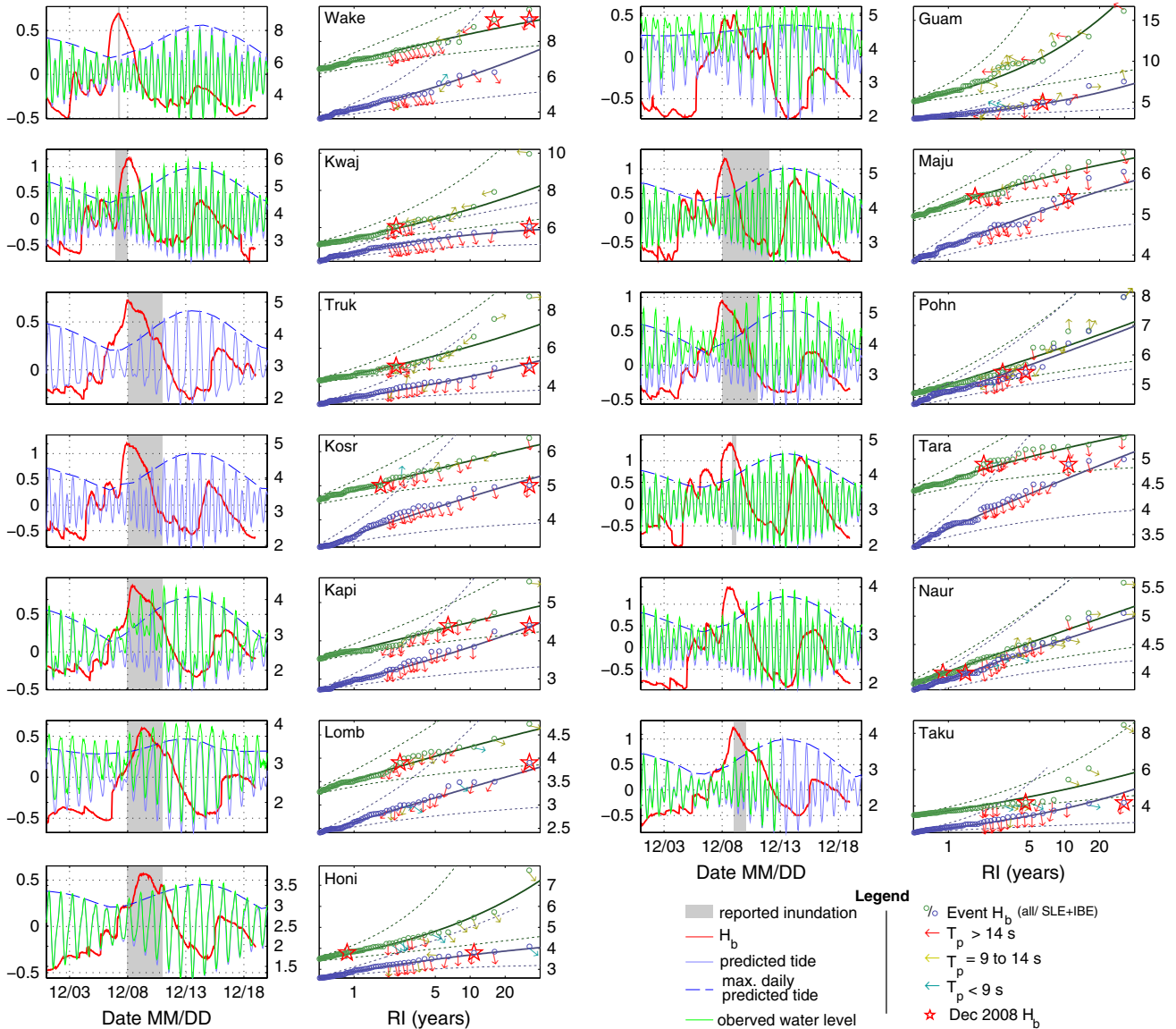

Fig. 3. Time-series comparison of estimated maximum wave height before breaking (H_b), predicted astronomic tides and observed water levels (primarily from tide gauges, see * below) at selected locations for the month of December, 2008 with observed water levels, predicted tides, and maximum daily predicted tidal envelope (max. daily tide) indicated on the left-hand axes and H_b values indicated on the right-hand axes (left hand plots). Corresponding empirical return intervals (RIs) of 99-percentile H_b event maxima are shown in the plot immediately to the right where four letter codes in bold indicate the locations of both respective plots and are defined in Table 1. The RIs of maximum event H_b are given with green circles; the RIs of the co-occurrence H_b and monthly sea level anomaly and inverse barometer effect ($SLA + IBE$ with trend) above a threshold value close to that of December 2008 are given with blue circles (see legend). For both sets of RIs, the largest event during December 2008 is highlighted with a red star; the date and time of this maximum event H_b can be found in Table 1 (note that at Guam, H_b during December 2008 was not in the tail of distribution of all events, so no red star is plotted). For RIs greater than two years, the peak direction of wave propagation (D_p) associated with each event is indicated with an arrow; color coding of the arrow indicates the associated peak period (T_p). The maximum likelihood generalized Pareto fit for all H_b events and for H_b events co-occurring with $SLA + IBE$ above the threshold are given with a green and purple line, respectively. 95% confidence limits for the fits are given with dotted lines. *No tide gauge data is available for "Taku" and "Kosr" and the "Truk" tide gauge was decommissioned around 1990. Observed water levels at "Taku" are derived from a pressure sensor deployed by J. Hunter and S. Smithers for a three week period. Tidal prediction for these locations is from the TPX7.2 global tidal model.

islands of Wake Atoll (Fig. 1a) and atolls in the Republic of the Marshall Islands (RMI) including Majuro, Kwajalein and Arno (Fig. 1b). This resulted in major infrastructure damage, clean-up efforts and remedial (Kosrae) and a national state of emergency was declared. In Papua New Guinea (PNG) and the Solomon Islands (SI), reported impacts commenced on December 8 and included 63,000 people affected and 1408 shore protection at several locations. More than 1500 km southeast of Wake, significant crop destruction and infrastructure damage were reported in all four states of Federated States of Micronesia (FSM; Chuuk, Pohnpei, Yap) houses damaged across 8 provinces of PNG (Fig. 1c) and heavy damage to crops and homes on atolls of Malaita Province (SI). Serious inundation was also reported in the Kiribati atoll of Marakei on December 9. All reports indicate that extreme water levels, high waves and associated island inundation and overwash had ceased by December 12 (UTC time), possibly earlier due to delays in reporting that may have occurred (Kruke and Olsen, 2012). Fig. 2 illustrates the wide area, approximately 3000 km in diameter, in which about 100,000 people were affected (a significant portion of the region's population), with millions of dollars in damage to infrastructure and unknown longer-term impacts on livelihoods, food security and freshwater resources, which can be slow to recover from inundation events (Terry and Chui, 2012).

The timing and severity of inundations at representative locations (Fig. 2) are summarized in Table 1. Astronomical tides, non-tidal residuals [sea level anomaly (SLA) and inverse barometer effect (IBE)], near-surface winds and wave re-analysis parameters [breaking wave height (H_b), peak period (T_p), peak direction (D_p) and maximum estimated wave set-up] are also summarized to evaluate their potential contributions to the extreme sea level.

The timing of maximum H_b (coincident with maximum wave energy flux (EC_g) in Fig. 2) corresponds to the reported onset of inundation to within about a day (sometimes within hours) at all locations (Table 1), generally occurring at the semi-diurnal high tide closest to maximum H_b (Fig. 3). Wave characteristics associated with the arrival of peak H_b (and EC_g) were that of swell (Barber and Ursell, 1948; Delpey et al., 2010), and the values of T_p and D_p place the origin of the swell between December 3–6 and 22–45°N. This time period and region coincides with

Table 2
Predicted maximum daily astronomical tidal percentiles (with heights in meters relative to MHHW in parentheses) at affected locations (from Table 1) on days with reported inundation. Tidal percentiles and heights are derived from an 18.6 prediction from the year 1992 to 2010. Asterisks following location codes in column one have the same meaning as in Table 1.

Loc	Dec07	Dec08	Dec09	Dec10	Dec11
Wake***	13.5 (−0.139)				
Kwaj***	21.6 (−0.213)	25.7 (−0.184)			
Maju**		24.8 (−0.199)	41.9 (−0.051)	60.4 (0.097)	84.2 (0.242)
Truk**		32.6 (−0.068)	57.7 (0.021)	82.3 (0.116)	95.9 (0.192)
Pohn**		28.6 (−0.125)	44.4 (−0.021)	68.4 (0.108)	91.8 (0.230)
Kosr**		26.6 (−0.180)	43.9 (−0.027)	63.4 (0.116)	88.2 (0.258)
Kapi***		30.8 (−0.095)	55.5 (0.032)	81.2 (0.151)	95.9 (0.247)
Tara*		47.4 (−0.005)			
Lomb***		74.2 (0.049)	87.6 (0.084)	96.1 (0.130)	99.0 (0.171)
Taku***			53.4 (0.041)	78.7 (0.181)	92.5 (0.281)
Honi**		40.0 (-0.024)	61.8 (0.022)	81.4 (0.070)	93.6 (0.113)

two mid-latitude cyclones, both of which reached hurricane force and developed long fetches directed towards the areas affected (Fig. 4).

Many of the reports listed in Supplementary Table S1 infer that unusually high tides (spring tides close to their astronomical maximum) contributed to the severity of the event. Tidal analysis shows that the highest perigean spring tides of the year did occur in December at several representative locations (see Supplementary Information S4). However, reported dates indicate inundation (and peak H_b) arrived prior to the peak spring tide by 3–5 days, when tides were roughly midway between neap and spring (Fig. 3). Table 2 lists the maximum daily predicted tidal heights above MHHW and percentiles during days of reported inundation. All locations (with the exception of one) experienced tides below MHHW (~50th percentile) at the reported onset of inundation. Over the next several days, the tides waxed towards the December perigean spring tidal maxima, reaching close to or greater than 90 percentile daily maximum heights during the last days of reported inundation. This suggests that astronomical tides may have contributed to the severity of inundation experienced at
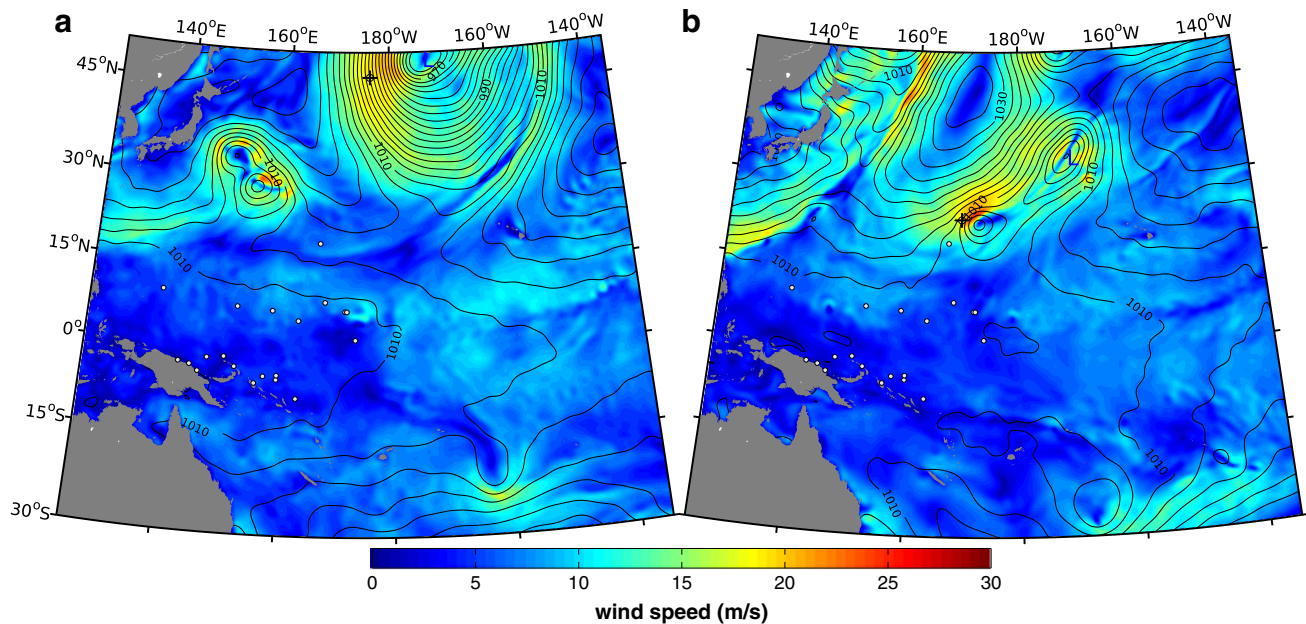

Fig. 4. Two north Pacific storms implicated by D_p and T_p associated with the arrival of maximum EC_g, as represented by CFSR surface pressure (contours, in hPa) and 10-height wind speed magnitude (colors, in m/s): (a) 18:00 December 3, 2008 and (b) 18:00 December 6, 2008 (b). These storms attained minimum pressures of 957.7 and 990.9 hPa, respectively, and both attained hurricane force winds in the CSFR reanalysis. Both had long fetches oriented towards the locations of the inundation events (white circles, Table 1). The black cross near the center of low pressure in both storms indicate the two "point source" locations calculated, see Supplementary Information S4 for more information.
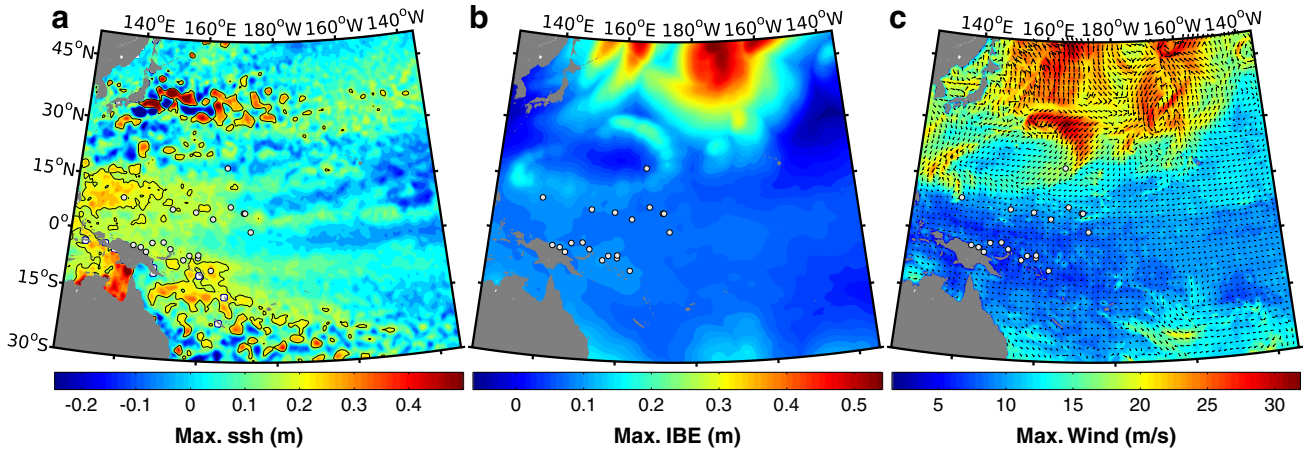
Fig. 5. Other non-tidal drivers of local sea level: (a) Maximum observed sea level anomaly (*SLA*), regions with *SLA* > 0.2 m are enclosed in a black contour line; (b) Maximum inverse barometer effect (IBE); and (c) maximum CFSR wind speed magnitude (colors) and vectors, wind vectors were re-sampled to 1.5° latitude resolution for legibility. In all plots, the values plotted are the maximum single value (peak value over the calendar month) of December 2008 at each point; locations with reported inundation for this period (Table 1) are indicated with white circles.

locations south of Wake and Kwajalein, particularly in PNG and SI, where relatively higher percentile daily maxima tides occurred some-what closer in time to the arrival of H_b (Fig. 3). It should be noted how-ever that the reports indicate that inundation had ceased at all locations days before the peak in spring tides, which occurred between December 13 and 15 at all locations.

Consistent with the ENSO conditions during December 2008 (weakly La Niña, MEI = −0.67), regional *SLA* was generally elevated (by 0.07–0.17 m in PNG, SI and FSM, Fig. 5a) and climatologically low regional atmospheric pressures further elevated sea levels (*IBE* of 0.02–0.04 m in RMI, FSM, SI and PNG). Low surface pressure gradients and light winds indicate that *IBE* at these locations were not associated with local storm conditions (Table 1, Fig. 5b–c).

Table 3
Estimated (empirical) probabilities (P) and return intervals (RI) of the December 2008 event. The first two columns show P and RI of the maximum estimated breaking wave height (H_b) alone, respectively. The next columns show P and RI of the co-occurrence of H_b and combined sea level anomaly and inverse barometer effect (*SLA + IBE*) with and without secular trends, respectively. Asterisks following location codes in column one have the same meaning as in Table 1.

Loc	Max. H_b		SLA + IBE (detrended)		SLA + IBE	
	P	RI	P	RI	P	RI
Wake***	0.01	16.0	0.02	16.0	0.01	32.0
Guam			0.33	0.9	0.07	5.4
Kwaj***	0.09	2.3	0.03	8.1	0.01	32.0
Maju**	0.13	1.7	0.06	3.6	0.04	8.1
Truk**	0.10	2.3	0.03	8.1	0.01	32.0
Pohn**	0.08	2.9	0.03	11.0	0.02	16.0
Kosr**	0.13	1.7	0.07	4.0	0.01	32.0
Kapi***	0.11	2.0	0.08	3.6	0.01	32.0
Tara*	0.04	6.5	0.04	8.1	0.03	11.0
Naur	0.27	0.9	0.20	1.2	0.15	1.8
Lomb***	0.12	2.5	0.09	3.6	0.01	32.0
Taku***	0.06	4.6	0.05	6.5	0.01	32.0
Honi**	0.28	0.9	0.21	1.3	0.03	11.0

The timing of the inundations clearly implicates the arrival of extra-tropical storm swell. The potential for inundation from swell is due to the steep bathymetric profiles of all affected locations. Unlike continental shelves, where depth-induced wave breaking (dissipation) tends to occur further from shore, steep bathymetry results in high dissipation gradients close to the coast resulting in more extreme wave set-up and run-up (Kennedy et al., 2012). Although our simplified treatment of wave-water level forcing does not include local spatial variation or explicit wave run-up, the calculated maximum set-up estimates of 0.75–1.85 m (Table 1) are consistent with many of the reported inundation levels, and are significantly greater than the sum of *SLA* and *IBE*, or any observed tidal residuals.

With the exception of Wake, return intervals (RIs) of maximum H_b during the December 2008 event are on the order of 4 yr, illustrating that long-period north swells of this magnitude are not particularly unusual (Fig. 3). However, if co-occurrence (joint probability) of maximum H_b and de-trended local monthly sea level (*SLA + IBE*) equal to or greater than that of December 2008 are considered, RIs are raised to 5–10 yr (Table 3). Furthermore, if the secular trend in sea level is included, RIs become 32 yr (the maximum that can be calculated from the hindcast) at all locations that reported severe dam-age (Fig. 3, Table 1). For Guam and Nauru, which reported no damage but experienced *SLA + IBE* similar to severely affected locations, RI for maximum December 2008 H_b was considerably shorter (Fig. 3). For example, the probability of an H_b event similar to December 2008 is about the same at Nauru and Honiara (about 1 yr RI); however the joint probability of both an H_b event and *SLA + IBE* similar to December 2008 has a RI of 1.8 yr at Nauru and 11 yr at Honiara. Nauru reported no significant damage, while major infrastructure damage and crop loss were reported in SI. This indicates that the regionally elevated sea levels created conditions that allowed a relatively common wave event to trigger damaging inundation, particularly at the more equatorial loca-tions (SI and PNG), although caution should be used when making com-parisons based on these attributes alone, as vulnerabilities are location specific and depend largely on coastal morphology and asset siting. *SLA + IBE* are strongly correlated with ENSO (Church et al., 2006; Walsh et al., 2012) in the region (R > 0.66, p < 0.001 at all locations except Wake, Tarawa, and Nauru in this study), with much higher (lower) *SLA + IBE* in the western (eastern) Pacific during La Niña conditions. However, while other studies have found links between wave climate and ENSO farther east and at higher latitudes (Bromirski et al., 2005; Aucan et al., 2012), we found no significant correlation (R < 0.2, p > 0.2) between the annual number of H_b events above the 99-percentile and MEI at all affected locations (undoubtedly
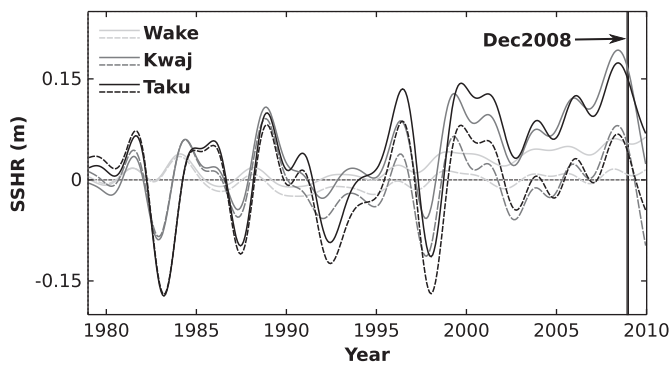
Fig. 6. Sea-surface height reconstruction (*SSHR*) timeseries including trends (solid) and with quadratic trends removed (dashed) for selected locations: Wake, Kwajalein (Kwaj) and Takuu (Taku). The latter two locations experience significant correlation between *SSHR* and ENSO (r > 0.8). The data have been smoothed with a 16-month low-pass filter to ease interpretation.

connections may exist, but researching these in detail are beyond the scope of this study). Therefore the lower probability of H_b events co-occurring with positive *SLA* appears to be statistically independent of ENSO (and is treated as such here), and therefore produces a far lower joint probability of H_b events above the 99-percentile with high regional *SLA + IBE*. This is due to the lower frequency of occurrence of La Nina compared to the combined frequency of ENSO neutral and El Niño conditions.

The secular trend in the sea level data has a large effect on the joint probability. Resulting RIs of co-occurrence events H_b and *SLA + IBE* similar to December 2008 are around 5–10 yr at affected locations, compared to 20–32 yr when the trend is included (Table 3). This is easily visualized by inspecting the reconstructed sea level (*SSHR ≈ SLA + IBE*) timeseries with and without trends (Fig. 6) at affected locations with a strong ENSO sea level response. In the de-trended timeseries, monthly sea levels are higher during previous, La Nina conditions, such as in 1988–1989 and 1999–2000 than during the (relatively weaker) La Nina conditions of 2008. However, if the trend is included the highest sea level in the *SSHR* record occurs in 2008 at most affected locations. This implies that accelerated SLR over the last two decades in the region (Merrifield, 2011), in addition to ENSO variability, was a significant contributor to the severity of this event.

4. Discussion and conclusions

Our analysis has shown that the December 2008 inundation event was caused primarily by remotely generated swell waves, but the severity was greatly increased by anomalously high regional sea levels linked with ENSO and SLR. The impact of this event would have been still greater had other sea level drivers also been more extreme (e.g. if such high wave energy had arrived during the peak of spring tides and stronger La Niña conditions). The exact contribution by astronomical tides is somewhat difficult to ascertain at most locations, due primarily to inconsistencies in reporting. Predicted tidal daily maxima were below or near average at the (reported) onset of inundation and (reported) inundation ceased several days before the perigian spring tidal maxima. The onset of inundation during below-average tides suggests that they contributed little to the severity of inundation; however tidal maxima were never-the-less near or above the 90th percentile height at southern locations at the end of (reported) inundation (Table 2). Due to the aforementioned delays in reporting, some doubts remain as to whether inundation was still actually occurring at these later dates, however these higher tides (relative to MHHW) may have exacerbated the length of inundation or recovery from it, particularly in PNG and SI. In one case at least (Takuu, PNG) the worst inundation occurred at high tide on December 10, one day after the arrival of

maximum H_b, when (predicted) tidal heights were approximately 18 cm above MHHW. This illustrates the important role tides may have played with regard to the exact timing of inundation and the potentially complex interaction between wave set-up and tidal heights, which our simple scaling of H_b as an estimate of wave set-up is unable to capture. This also highlights the importance of improved reporting: such processes can be much better elucidated when the exact timing and severity (i.e. estimated still water heights and horizontal extent of inundation) are recorded. This was done to some degree in only 3 of more than 28 reports reviewed for this study.

In terms of causality, however, it should be noted that the periodic nature of tides makes them a stationary, statistically short-tailed phenomena: 90th percentile tidal heights or greater occur regularly ~36 days annually, whereas the stochastic nature of swell wave events makes them a random long-tailed phenomena. The maximum H_b associated with the December 2008 events have occurred only a handful of times (in some cases only once) in the entire 30-year hindcast record. So while tides certainly modulated inundation and impacts within the timescale of reporting, given the timing of the reported inundation events, they did not "cause" inundation and their contribution is difficult or impossible to elucidate without better reporting and/or direct geophysical observations (instrumentation) at the affected locations.

A more robust and arguably more important result is the implication of recent (in the last ~20 yr) non-ENSO related accelerated SLR in the region (Merrifield, 2011), e.g. note the difference in RIs at affected locations with and without secular trends (Table 3 and Fig. 6). This suggests that the predictions of increasing impact of climate change related SLR (e.g. Nicholls et al., 2007; Walsh et al., 2012) may already be coming to the fore in the region, although whether this recent accelerated SLR is attributable to (anthropogenic) climate change or decadal climate variability is difficult to determine (Zhang and Church, 2012) and beyond the scope of this work. Changes in wave climate may also have a large impact on the future frequency and severity of such events. While these changes remain uncertain, current trends in storm wave height and frequency, particularly in the mid- and high-latitudes, tend to be positive (Bromirski et al., 2005; Young et al., 2011; Aucan et al., 2012; Hemer et al., 2013). Regardless, future swell wave events of similar magnitude to that described here will more frequently achieve similar or greater impacts in the region under all SLR projections for the next century.

It should not be overlooked that the region's tide gauges did not capture the extreme water levels associated with the inundation. The reason is that although tide gauges respond to wave set-up and very occasionally offer a good record of it (e.g. Aucan et al., 2012), almost all are sited in sheltered locations such as harbors, and this, combined with the large local gradients in wave set-up, means they usually do not capture this localized contribution (Thompson and Hamon, 1980). For example, Tarawa recorded a residual of 22 cm above *SLA + IBE* at the time of high H_b but reported water levels indicate it was at least twice this in affected areas. Other tide gauges, such as at Majuro, show minimal signs of wave set-up despite significant impacts nearby (Fig. 1, Table 1). Furthermore, high wave set-up is generally accompanied by high wave run-up, energetic near-shore currents and possibly complex nonlinear effects such as infra-gravity waves, all which may greatly exacerbate inundation, damage to coastal infrastructure and other impacts. Divergence between actual local extreme water levels and those recorded by tide gauges has almost certainly confounded awareness and understanding of the causes and risks of inundation events, especially those generated by distant-source waves.

The events reported here are by no means unprecedented. In November and December 1979 severe inundation occurred in RMI (over 5000 people lost their homes); in April 1987 flooding of over a meter occurred in the Maldives with significant damage to property and sea defenses (Harangozo, 1992), in 1999, north Atlantic swell coincided with spring tides at Ascension and St Helena Islands south of the Equator (Vassie et al., 2004) and in May 2011 damaging flooding

occurred along the southern coast of Viti Levu, Fiji (Supplementary Table S3). Swells generated by either northern or southern hemisphere mid-latitude storms are implicated in these events; many other swell-driven events (perhaps of lesser impact) surely have occurred, but been unreported or misreported. These additional examples indicate that the findings presented here have import outside the western Pacific region: distant storm systems are important when assessing risks to island populations. While tide gauges provide invaluable insight into sea level variability and rise, they are not a reliable source of information about extreme sea levels associated with wave set-up and run-up. The lack of systematic in situ wave and water level measurements in wave-exposed areas across the region causes a reliance on tide gauge data to understand the causes of extreme sea levels, perpetuating an incomplete understanding of the significant (and most likely increasing) risk caused by remotely-generated swell to the communities of low-lying areas in island nations.

Clearly, if island climate change adaptation and related disaster mitigation strategies are to be effective, the role of waves in extreme sea level events needs to be better understood. A number of questions emerge from the work presented here: What are the storm track and intensity characteristics associated with inundation at a particular (set of) island(s)? What combination of waves, tides, and regional sea level anomaly produce the most severe impacts? How will the severity and frequency of events such as those reported here change over time at any given location? Answers to these questions are needed to project impacts with accuracy. This requires increasing in situ observations of coastal wave and sea levels and better morphological (e.g. bathymetry, topography and shoreline position) information, as well as greater detail and standardization of coastal inundation reporting for oceanic islands. For example, there is currently only one operational wave buoy in the Pacific islands (excluding developed Pacific rim countries and Hawaii), located near Guam. This is also the only wave buoy in the region to have recorded more than one year of continuous data. Shallow water bathymetric and nearshore topographic information, such as provided by Light Detection and Ranging (LiDaR), is non-existent for most Pacific island nations. While high logistical and operational costs of data collection are the main causes for the limited data availability in the region, even a limited expansion of in situ observations and other information could be combined with improved numerical simulation techniques to decrease current shortcomings in prediction of impacts. For instance, the integration of operational wave models (Tolman et al., 2011) and forecasts of ENSO-related sea-level may well provide skillful early-warnings of future events.

Beyond the direct impacts of single events highlighted above, more frequent and severe wave-driven inundation events will have a number of longer-term impacts. These include long-term impacts on coastal groundwater (Terry and Chui, 2012), even considerable distance from the coast (Rotzoll and Fletcher, 2013); rapid dynamic geomorphic response of islands, e.g. shifts in erosion and sedimentation rates and patterns (Webb and Kench, 2010); coastal ecosystem shifts (e.g. Storlazzi et al., 2011); and perhaps unforeseen synergistic effects between these processes (e.g. Perry et al., 2011). Indeed it is likely that the limits to adaptation and possibly habitability on many low-lying islands will be defined by the changes in the occurrence of these episodic events more than progressively rising sea levels.

Acknowledgments

Appendix A. Supplementary data

Supplementary data to this article can be found online at http://dx.doi.org/10.1016/j.gloplacha.2013.06.006.

References

Aucan, J., Hoeke, R., Merrifield, M.A., 2012. Wave-driven sea level anomalies at the Midway tide gauge as an index of North Pacific storminess over the past 60 years. Geophysical Research Letters 39 (17).

Barber, N.F., Ursell, F., 1948. The generation and propagation of ocean waves and swell. I. Wave periods and velocities. Philosophical Transactions of the Royal Society of London, Series A, Mathematical and Physical Sciences 240 (824), 527–560.

Barnett, J., 2011. Dangerous climate change in the Pacific islands: food production and food security. Regional Environmental Change 11 (1), 229–237.

Bromirski, P.D., Cayan, D.R., Flick, R.E., 2005. Wave spectral energy variability in the northeast Pacific. Journal of Geophysical Research 110.

Caldwell, P.C., Aucan, J.P., 2007. An empirical method for estimating surf heights from deep-water significant wave heights and peak periods in coastal zones with narrow shelves, steep bottom slopes, and high refraction. Journal of Coastal Research 1237–1244.

Callaghan, D.P., Nielsen, P., Cartwright, N., Gourlay, M.R., Baldock, T.E., 2006. Atoll lagoon flushing forced by waves. Coastal Engineering 53 (8), 691–704.

Church, J., White, N., 2011. Sea-level rise from the late 19th to the early 21st century. Surveys in Geophysics 32 (4–5), 585–602.

Church, J.A., White, N.J., Coleman, R., Lambeck, K., Mitrovica, J.X., 2004. Estimates of the regional distribution of sea level rise over the 1950, 2000 period. Journal of Climate 17 (13), 2609–2625.

Church, J.A., White, N.J., Hunter, J.R., 2006. Sea-level rise at tropical Pacific and Indian Ocean islands. Global and Planetary Change 53 (3), 155–168.

Codiga, D.L., 2011. Unified Tidal Analysis and Prediction Using the UTide Matlab Functions. Graduate School of Oceanography, University of Rhode Island, Narragansett, RI.

Dean, R.G., Dalrymple, R.A., 1984. Water Wave Mechanics for Engineers and Scientists/ Robert G. Dean, Robert A. Dalrymple. Prentice-Hall, Englewood Cliffs, N.J.

Delpey, M.T., Ardhuin, F., Collard, F., Chapron, B., 2010. Space-time structure of long ocean swell fields. Journal of Geophysical Research 115 (C12), C12037.

Egbert, G.D., Erofeeva, S.Y., 2002. Efficient inverse modeling of barotropic ocean tides. Journal of Atmospheric and Oceanic Technology 19 (2), 183–204.

Filipot, J.-F., Cheung, K.F., 2012. Spectral wave modeling in fringing reef environments. Coastal Engineering 67, 67–79.

Gourlay, M.R., Colleter, G., 2005. Wave-generated flow on coral reefs—an analysis for two-dimensional horizontal reef-tops with steep faces. Coastal Engineering 52 (4), 353–387.

Harangozo, S.A., 1992. Flooding in the Maldives and its implications for the global sea level rise debate. In: Woodworth, P.L., Pugh, D.T., DeRonde, J.G., Warrick, R.G., Hannah, J. (Eds.), Sea Level Changes: Determination and Effects. American Geophysical Union, pp. 95–99.

Hemer, M.A., Katzfey, J., Trenham, C.E., 2013. Global dynamical projections of surface ocean wave climate for a future high greenhouse gas emission scenario. Ocean Modelling (0) (in press).

Holthuijsen, L.H., 2007. Waves in Oceanic and Coastal Waters. Cambridge University Press, Cambridge.

Kennedy, A.B., Westerink, J.J., Smith, J.M., Hope, M.E., Hartman, M., Taflanidis, A.A., Tanaka, S., Westerink, H., Cheung, K.F., Smith, T., Hamann, M., Minamide, M., Ota, A., Dawson, C., 2012. Tropical cyclone inundation potential on the Hawaiian Islands of Oahu and Kauai. Ocean Modelling 52-i53 (0), 54–68.

Kruke, B.I., Olsen, O.E., 2012. Knowledge creation and reliable decision-making in complex emergencies. Disasters 36 (2), 212–232.

Longuet-Higgins, M.S., Stewart, R.W., 1964. Radiation stresses in water waves; a physical discussion, with applications. Deep Sea Research 11, 529–562.

Lowe, R.J., Falter, J.L., Bandet, M.D., Pawlak, G., Atkinson, M.J., Monismith, S.G., Koseff, J.R., 2005. Spectral wave dissipation over a barrier reef. Journal of Geophysical Research 110, 16.

Lowe, R.J., Falter, J.L., Monismith, S.G., Atkinson, M.J., 2009. Wave-driven circulation of a coastal reef–lagoon system. Journal of Physical Oceanography 39 (4), 873–893.

Lowe, J.A., Woodworth, P.L., Knutson, T., McDonald, R.E., McInnes, K.L., Woth, K., von Storch, H., Wolf, J., Swail, V., Bernier, N.B., Gulev, S., Horsburgh, K.J., Unnikrishnan, A.S., Hunter, J.R., Weisse, R., 2010. Past and Future Changes in Extreme Sea Levels and Waves, Understanding Sea-Level Rise and Variability. Wiley-Blackwell 326–375.

Menéndez, M., Woodworth, P.L., 2010. Changes in extreme high water levels based on a quasi-global tide-gauge data set. Journal of Geophysical Research: Oceans 115 (C10), C10011.

Merrifield, M.A., 2011. A shift in western tropical pacific sea level trends during the 1990s. Journal of Climate 24 (15), 4126–4138.

Munk, W., Sargent, M., 1948. Adjustment of Bikini Atoll to waves. Transactions American Geophysical Union 29 (6), 855–860.

Munk, W.H., Miller, G.R., Snodgrass, F.E., Barber, N.F., 1963. Directional recording of swell from distant storms. Philosophical Transactions of the Royal Society of London, Series A, Mathematical and Physical Sciences 255 (1062), 505–584.

Nicholls, R.J., Wong, P.P., Burkett, V.R., Codignotto, J.O., Hay, J.E., McLean, R.F., Ragoonaden, S., Woodroffe, C.D., 2007. Coastal systems and low-lying areas. In: Parry, M.L., Canziani, O.F., Palutikof, J.P., Linden, P.J.V.D., Hanson, C.E. (Eds.), Climate Change 2007. Impacts, Adaptation and Vulnerability. Contribution of Working Group II to the Fourth Assessment Report of the Intergovernmental Panel on Climate Change. Cambridge University Press, Cambridge, UK, pp. 315–356.

OCHA U.N., 2011. Protecting the Human Rights of Internally Displaced Persons in Natural Disasters: Challenges in the Pacific. U.N. Office of the High Commissioner for Human Rights (OHCHR), Suva, Fiji.

Perry, C.T., Kench, P.S., Smithers, S.G., Riegl, B., Yamano, H., O'Leary, M.J., 2011. Implications of reef ecosystem change for the stability and maintenance of coral reef islands. Global Change Biology 17 (12), 3679–3696.

Pomeroy, A., Lowe, R., Symonds, G., Van Dongeren, A., Moore, C., 2012. The dynamics of infragravity wave transformation over a fringing reef. Journal of Geophysical Research: Oceans 117 (C11), C11022.

Rotzoll, K., Fletcher, C.H., 2013. Assessment of groundwater inundation as a consequence of sea-level rise. Nature Climate Change 3 (5), 477–481.

Saha, S., Moorthi, S., Pan, H.-L., Wu, X., Wang, J., Nadiga, S., Tripp, P., Kistler, R., Woollen, J., Behringer, D., Liu, H., Stokes, D., Grumbine, R., Gayno, G., Wang, J., Hou, Y.-T., Chuang, H.-Y., Juang, H.-M.H., Sela, J., Iredell, M., Treadon, R., Kleist, D., Van Delst, P., Keyser, D., Derber, J., Ek, M., Meng, J., Wei, H., Yang, R., Lord, S., Van Den Dool, H., Kumar, A., Wang, W., Long, C., Chelliah, M., Xue, Y., Huang, B., Schemm, J.-K., Ebisuzaki, W., Lin, R., Xie, P., Chen, M., Zhou, S., Higgins, W., Zou, C.-Z., Liu, Q., Chen, Y., Han, Y., Cucurull, L., Reynolds, R.W., Rutledge, G., Goldberg, M., 2010. The NCEP climate forecast system reanalysis. Bulletin of the American Meteorological Society 91 (8), 1015–1057.

Seneviratne, S.I., Nicholls, N., Easterling, D., Goodess, C.M., Kanae, S., Kossin, J., Luo, Y., Marengo, J., McInnes, K., Rahimi, M., Reichstein, M., Sorteberg, A., Vera, C., Zhang, X., 2012. Changes in climate extremes and their impacts on the natural physical environment. In: Field, C.B., Barros, V., Stocker, T.F., Qin, D., Dokken, D., Ebi, K.L., Mastrandrea, M.D., Mach, K.J., Plattner, G.-K., Allen, S.K., Tignor, M., Midgley, P.M. (Eds.), Intergovernmental Panel on Climate Change Special Report onManaging the Risks of Extreme Events and Disasters to Advance Climate Change Adaptation. Cambridge University Press, Cambridge, United Kingdom and New York, NY, USA.

Storlazzi, C.D., Elias, E., Field, M.E., Presto, M.K., 2011. Numerical modeling of the impact of sea-level rise on fringing coral reef hydrodynamics and sediment transport. Coral Reefs 30 (1), 83–96.

Taebi, S., Lowe, R., Pattiaratchi, C., Ivey, G., Symonds, G., 2012. A numerical study of the dynamics of the wave-driven circulation within a fringing reef system. Ocean Dynamics 62 (4), 585–602.

Tait, R.J., 1972. Wave set-up on coral reefs. Journal of Geophysical Research 77 (12), 2207–2211.

Terry, J.P., Chui, T.F.M., 2012. Evaluating the fate of freshwater lenses on atoll islands after eustatic sea-level rise and cyclone-driven inundation: a modelling approach. Global and Planetary Change 88–89, 76–84.

Thompson, R.O.R.Y., Hamon, B.V., 1980. Wave setup of harbor water levels. Journal of Geophysical Research 85 (C2), 1151–1152.

Tolman, H.L., 2009. User Manual and System Documentation of WaveWatch III Version 3.14. Tech. Note 276, NOAA/NWS/NCEP/MMAB.

Tolman, H., Banner, M., Kaihatu, J., 2011. The NOPP operational wave improvement project. Proceedings, 12th Int. Workshop of Wave Hindcasting and Forecasting, Hawaii, Kohala Coast, Hawai'i, HI, pp. 1–19.

Vassie, J.M., Woodworth, P.L., Holt, M.W., 2004. An example of north Atlantic deep-ocean swell impacting Ascension and St. Helena Islands in the Central South Atlantic. Journal of Atmospheric and Oceanic Technology 21 (7), 1095–1103.

Vetter, O., Becker, J.M., Merrifield, M.A., Pequignet, A.C., Aucan, J., Boc, S.J., Pollock, C.E., 2010. Wave setup over a Pacific Island fringing reef. Journal of Geophysical Research 115 (C12), C12066.

Walsh, K.J.E., McInnes, K.L., McBride, J.L., 2012. Climate change impacts on tropical cyclones and extreme sea levels in the South Pacific — a regional assessment. Global and Planetary Change (0), 149–164.

Webb, A.P., Kench, P.S., 2010. The dynamic response of reef islands to sea-level rise: evidence from multi-decadal analysis of island change in the Central Pacific. Global and Planetary Change 72 (3), 234–246.

Wolter, K., Timlin, M.S., 1998. Measuring the strength of ENSO events — how does 1997/98 rank? Weather 53, 315–324.

Young, I.R., Zieger, S., Babanin, A.V., 2011. Global trends in wind speed and wave height. Science 332 (6028), 451–455.

Zhang, X., Church, J.A., 2012. Sea level trends, interannual and decadal variability in the Pacific Ocean. Geophysical Research Letters 39 (21) (n/a–n/a).